Evapotranspiration Derived from Satellite Observed Surface Temperatures

Klaassen, Wim; Berg, Wim van den

Published in:
Journal of Climate and Applied Meteorology

DOI:
10.1175/1520-0450(1985)024<0412:EDFSOS>2.0.CO;2

Publication date:
1985

Evapotranspiration Derived from Satellite Observed Surface Temperatures

WIM KLAASSEN[1] AND WIM VAN DEN BERG

Institute for Meteorology and Oceanography, Princetonplein 5, University of Utrecht, The Netherlands

(Manuscript received 1 September 1984, in final form 20 December 1984)

ABSTRACT

Evapotranspiration is calculated from surface temperatures using an energy balance method. This method is sensitive to the temperature difference between the surface and the air above, and somewhat to the windspeed. In this study we consider the influence of the spatial variability of air temperature on the interpretation of surface temperatures.

It is argued that small-scale atmospheric variations can be corrected by using temperature and wind data at a height of 50 m. Three models have been used to calculate these 50 m data from standard weather observations. The first model uses a very simple concept of constant temperature and wind over the test area (zero-dimensional). In the second model windspeed is also taken constant, but air temperature is evaluated from the initial vertical temperature in the atmosphere with a one-dimensional slab layer model. The third model is a two-dimensional primitive equations model in which wind velocity is calculated from the geostrophic wind and air temperature similar to model 2.

A homogeneous grassland area was selected in the north of the Netherlands close to the sea. Several days in the summer of 1983 with clear skies and winds from the sea were selected. Surface temperatures were derived from the NOAA-7 satellite overpass in the early afternoon using the split-window technique. On most days an almost linear increase of both surface and air temperature is found with increasing distance to the sea.

This study reveals that model 1 results in an unrealistic decrease of the calculated evapotranspiration with increasing distance to the coast. Furthermore evapotranspiration is underestimated. The evapotranspiration as calculated with models 2 and 3 is almost constant in the test area and agrees well with measurements. Model 3 gave more scatter, probably due to the fact that uncalibrated wind velocities were used.

For practical calculation of evapotranspiration the Priestley–Taylor parameter α is often used. This study shows how this parameter can be derived from satellite observations of surface temperature.

1. Introduction

Evapotranspiration can be calculated from the energy balance at the surface. With this approach an estimation has to be made for the distribution of the available energy between sensible and latent heat. Several methods exist; they use a surface wetness constant, a supplementary resistance for water vapor transport or a Priestley–Taylor constant. These methods can result in large errors in cases of limited soil water availability. Calibration on point measurements is of restricted value only, since evapotranspiration depends on type of crop and soil, and supply of water.

Several authors use thermal infrared remote sensing techniques for the estimation of evapotranspiration or water stress (Bartholic *et al.*, 1972; Idso *et al.*, 1975; Soer, 1980; Price, 1982; England *et al.*, 1983; Gurney and Hall, 1983). These models are also based on the energy balance of the surface. Instead of assuming some water availability parameter, they use the temperature difference between the surface and the air above to calculate the sensible and latent heat fluxes. As air and surface temperatures are measured with different methods, the absolute value of the temperature difference is difficult to obtain. Therefore the remote sensing technique is often restricted to predict evapotranspiration differences rather than absolute values (Jackson *et al.*, 1977).

In this study however we will investigate the possibilities of calculating the absolute value of evapotranspiration from surface temperatures: with the installation of the split-window measurement technique (Prabhakara *et al.*, 1974) on recent satellites the atmospheric absorption of thermal radiation, and thus the surface temperature, can be estimated more accurately. Another possible error source is the air temperature. Although air temperature can be measured accurately, it will vary in a horizontal plane over nonhomogeneous surfaces. For the interpretation of thermal images horizontal air temperature variations are often ignored. It is the purpose of this paper to take these variations into account.

Modeling of air temperature for the interpretation

[1] Present address: Laboratory of Transmission of Information, Department of Electrical Engineering, Delft University of Technology, the Netherlands.

of surface temperatures is rather rare until now: Carlson *et al.* (1981) used a one-dimensional Eulerian slab model to calculate nocturnal cooling. One-dimensional Eulerian modeling is, in our opinion, suitable for time-dependent temperature variations, but not for areal variations. Then the Lagrangian approach of a vertical air column moving with the wind velocity seems to be more adequate. Lagrangian modeling has been used by to describe cold air outbreaks over warm water (Chou and Atlas, 1982; Stage, 1983). These authors use cloud information as input for the vertical profile of temperature and humidity. But in our cases with clear skies, we will use measured temperature and humidity profiles.

Recently, Wetzel *et al.* (1984) discussed the feasibility of using the increase of surface temperature in the morning. They state that two measurements of surface temperature may replace the measurement of the vertical temperature profile. Such a method is restricted by the poor resolution of geosynchronous satellites and to situations of limited advection.

For the interpretation of areal temperature differences, this study emphasizes that the fluxes should be calculated up to a height above the usual measurement height of air temperature. Three models with increasing degree of complexity are given to calculate temperature and wind at this height. The more complex models are used to verify the assumptions of the simpler models.

2. Methods

a. *Surface fluxes*

The evapotranspiration from the surface can be calculated indirectly from the surface temperature T_s by means of the energy balance. This approach has been discussed before by authors like Soer (1980) and Seguin and Itier (1983). To show the potentials and limitations of this approach, only the basic equations will be discussed in this section.

Evapotranspiration LE can be derived from the energy balance equation at the surface:

$$LE = Q - G - H \tag{1}$$

where Q is net radiation, G soil heat flux, H sensible heat flux and L latent heat of evaporation per unity of mass. To determine $Q - G$ we will follow the formulation given by Holtslag and van Ulden (1983) for grassland in the Netherlands (see Appendix).

The available energy $Q - G$ can be derived fairly accurately under clear sky conditions. The main problem is found in the partitioning of $Q - G$ into sensible and latent heat flux. For this problem surface temperatures can be used to calculate the sensible heat flux from:

$$H = \rho c_p C_H (T_s - T_a), \tag{2}$$

where ρ is air density, c_p specific heat capacity of air at constant pressure, C_H the heat exchange coefficient, T_s and T_a are surface and air temperature. The heat exchange coefficient is derived from the logarithmic profile by:

$$C_H^{-1} = [\ln(z/z_0)]^2/(s_h k^2 u) + r_v, \tag{3}$$

where z is reference height, discussed in Section 2b, z_0 the roughness length, here taken as $z_0 = 0.03$ m (Wieringa, 1980), s_h a stability correction for heat, k is von Karman's constant, here taken as $k = 0.4$, u the wind velocity at level z and r_v is an excessive resistance introduced by Thom (1972) resulting from the invalidity of the Reynolds analogy between momentum and heat transport close to the vegetated surface. The magnitude of r_v for remote sensing purposes is still not precisely known. In this study Thom's formulation is used, as Seguin and Itier (1983) found that its influence is about the average of other formulations. So:

$$r_v = 6.27 u_*^{-2/3} \tag{4}$$

where u_* is friction velocity, given by:

$$u_* = s_m k u/\ln(z/z_0), \tag{5}$$

where s_m is the stability correction for momentum exchange. For s_m and s_h the formulation of Louis (1979) is used. It is concluded that the heat exchange coefficient C_H is known with a fair accuracy. For small values of $T_s - T_a$, or high evapotranspiration, errors in C_H have only a small influence on H and LE. However, for drought situations the heat exchange coefficient needs to be known with higher accuracy.

According to Eq. (2) sensible heat flux is proportional to the temperature difference between the surface and the air above the surface. This temperature difference has to be known with a high accuracy of about 1°C for a useful determination of sensible and latent heat flux. With the split-window observation technique on recent satellites the rms error of surface temperatures has dropped below 1°C (McClain, 1980). Air temperature can be measured even more accurately; however, it is measured on a restricted number of places and may have horizontal variations of more than 1°C. Therefore air temperature variations (and wind velocity) are modeled in this study.

The partitioning of $Q - G$ in $H + LE$ can also be derived from the empirical Priestley–Taylor concept:

$$LE = \alpha(Q - G)/(1 + c_p L^{-1} s^{-1}) + \beta, \tag{6}$$

where $s = dq_s/dT$, the slope of saturation specific humidity with temperature, and α and β are empirical constants. Equation (6) shows that evapotranspiration is mainly determined by the available energy $Q - G$ and the soil water availability (through α and β; see Holtslag and van Ulden, 1983), while air temperature and wind velocity have a minor influence on LE.

This empirical fact will be used for the evaluation of the results of the satellite-derived evapotranspiration.

b. Air temperature and wind velocity

1) THE REFERENCE HEIGHT

Air temperature is normally measured at a height of 2 m. It is to be expected that at this height air temperature is affected by the fluxes at the underlying surface. The coupling between air temperature and surface fluxes decreases for increasing height. Therefore a high reference height is preferred. The problem is that the logarithmic profile [corrected for stability, Eqs. (3) and (5)] is only valid in a thin constant flux layer above the surface. To evaluate how these equations can be used up to a higher level we will analyze the structure of the lower atmosphere.

A picture of the lower atmosphere is shown in Fig. 1 to illustrate some concepts. Above the surface a thin constant flux layer develops. The height of this layer is up to ten percent of the fetch, i.e., the distance to the upwind step change at the surface (Pasquill, 1972). Temperature, humidity and wind velocity in the constant flux layer are related to the surface fluxes of sensible heat, latent heat and momentum through the logarithmic profile. At the top of the constant flux layer, mixing with air from the constant flux layer of the upwind surface takes place. As a result, the atmospheric properties above the lowest constant flux layer are related to the surface fluxes at a larger scale.

In an unstable atmosphere the vertical mixing increases with height above the surface. From a certain height, we may assume complete mixing and the mixed layer is formed. Deardorff (1972) suggests that this height should be taken proportional to the height of the mixed layer. By lack of verification and for simplicity we use a constant value of 50 m. Because of the complete mixing the potential temperature in the mixed layer is constant with height. Because of the large heat capacity of the mixed layer horizontal temperature gradients are also very small in this layer.

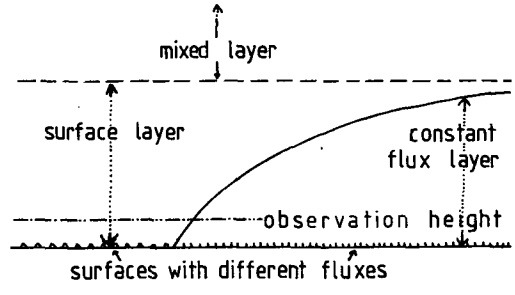

FIG. 1. Structure of the lower atmosphere near a step change at the surface.

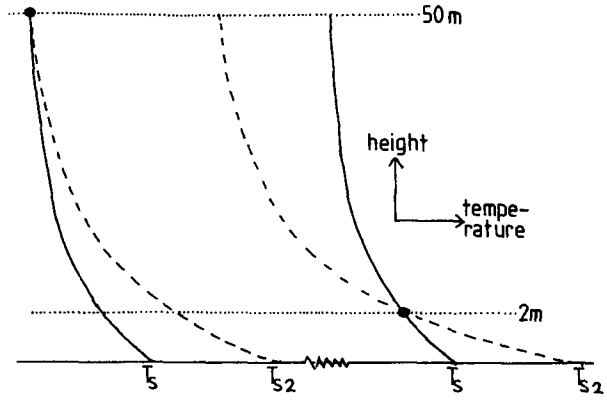

FIG. 2. Vertical temperature profiles in the surface layer resulting from two surface temperatures. In the left part a constant air temperature at 50 m height is assumed, and on the right at 2 m. The assumption of a constant air temperature at 2 m height results in strong temperature variations at 50 m height.

For an extended surface the constant flux layer will reach the mixed layer. In that case the air properties in the constant flux layer are determined by the logarithmic profiles up to the mixed layer. For small fetches the constant flux layer does not yet reach the mixed layer. In such situations surface temperature is found to be adapted within a few meters fetch to new environmental conditions (Klaassen and Nieuwenhuis, 1978). This implies that air temperature in the constant flux layer is almost independent of fetch. Thus even if the constant flux layer does not reach the mixed layer, the air properties in the constant flux layer can be derived from a logarithmic profile up to the mixed layer. This means that the reference height [Eq. (3)] should be set at the bottom of the mixed layer (here 50 m), instead of using the measurement height (2 m) as a reference height.

Elevating the reference height has considerable consequences for the flux calculations from surface temperatures. It was already shown by Klaassen (1980) that increasing the reference height improved the results of the calculation of evapotranspiration of crops, differing in surface roughness. For a constant surface roughness and varying heat fluxes the influence of the reference height is shown in Fig. 2. Assuming a constant air temperature at 2 m height would result in unrealistic temperature variations in the mixed layer. Further on the sensitivity of the sensible heat flux to variations in the surface temperature is changed: with $u_{2m} = 5$ m s^{-1}, $z_0 = 0.03$ m, neutral stability and constant air properties at 2 m height, the sensitivity of the sensible heat flux with surface temperature is calculated as $dH/dT_s = 37$ W m^{-2} K^{-1}, while a reference height of 50 m gives $dH/dT_s = 24$ W m^{-2} K^{-1}. In unstable atmospheres these differences are smaller and in stable atmospheres larger than given in this example. As a consequence

of the reduced sensitivity, the calculated fluxes are less influenced by measurement errors in the surface temperature given the air temperature at a high level.

2) MODEL 1

In model 1 constant air temperature and wind velocity are assumed at the reference height of 50 m. The 50 m data are calculated from the 2 m height measurements as follows:

At the meteorological station the fluxes of sensible heat [Eqs. (2)–(4)] and momentum [$\tau = \rho u_*^2$; Eq. 5] are calculated from the roughness length, wind velocity, air and surface temperatures. These fluxes are taken constant with height in the surface layer. As a result the air temperature and wind velocity at 50 m height are calculated using the same equations [(2)–(5)]. As the stability corrections s_h and s_m depend on height, this procedure is executed iteratively until *the 50 m data result in the same fluxes at the observation place* as the measurements.

3) MODEL 2

The principal distinction between models 1 and 2 is that model 2 does not assume a constant air temperature at reference height. The air temperature variations at 50 m and in the mixed layer are calculated with an one-dimensional Lagrangian model as described by Tennekes (1973) that applies to the unstable situation. A more general model for operational applications is described by Reiff *et al.* (1984).

In the mixed layer, potential temperature θ is taken as constant. By neglecting variation of advection with height and cooling by radiative divergence, the temperature in the mixed layer is given by

$$\frac{d\theta}{dt} = \frac{H + H_h}{\rho c_p h}, \tag{7}$$

where h is the height of the mixed layer. The sensible heat flux at the top of the mixed layer H_h is caused by conversion of kinetic energy to potential energy. The kinetic energy arises by surface heating and mechanical friction. Driedonks (1982) found

$$H_h = aH + b\frac{u_*^3 T_s}{\rho c_p g h} \tag{8}$$

with $a = 2$ and $b = 5$. Neglecting large-scale vertical motion, the increase with time of h is given by:

$$\frac{dh}{dt} = \frac{H_h}{\rho c_p \Delta\theta}, \tag{9}$$

where $\Delta\theta = \theta_h - \theta$, the temperature jump at the inversion at the top of the mixed layer. In our situation temperature variations parallel to the coast are neglected. The temperature variation perpendicular to the coast ($\partial\theta/\partial x$) is found with:

$$\frac{d\theta}{dt} = \frac{\partial\theta}{\partial x}\cdot\frac{\partial x}{\partial t} = \frac{\partial\theta}{\partial x}\cdot u_x, \tag{10}$$

where u_x is the wind component perpendicular to the coast.

Assuming a constant lapse rate ($d\theta/dz$) of the initial atmosphere, constant surface fluxes and $b = 0$ results in an increase of air and surface temperatures, and mixed-layer height with the square root of distance to the coast (Fig. 3). The mechanical friction term b results in an increased heat absorption in the mixed layer for low mixed-layer heights. This results in an increased linearity of temperature for small distances to the sea. Inland, a decrease of wind velocity is often found, resulting in an increase of the temperature difference between the surface and the air above. So Fig. 3 shows that a linear surface temperature increase is possible over a wide range of distances to the sea.

Instead of using the air temperature at 2 m height (model 1), model 2 uses the initial vertical temperature profile.

4) MODEL 3

Model 3 is similar to model 2, but now the wind velocity is variable and follows from a two-dimensional mesoscale model including a simplified energy balance equation. The model is a hydrostatic primitive equations model, based on the work of Anthes and Warner (1978). The horizontal axis x is chosen perpendicular to the coast and we introduce a relative pressure

$$\sigma = \frac{p - p_{\text{top}}}{p_{\text{surf}} - p_{\text{top}}} = \frac{p - p_{\text{top}}}{p_*}, \tag{11}$$

as vertical coordinate, where p_{top} is the pressure at the upper boundary of the model. We used a horizontal grid length of 6 km and a time step of 20 s. The model consists of 14 layers, of which 8 layers

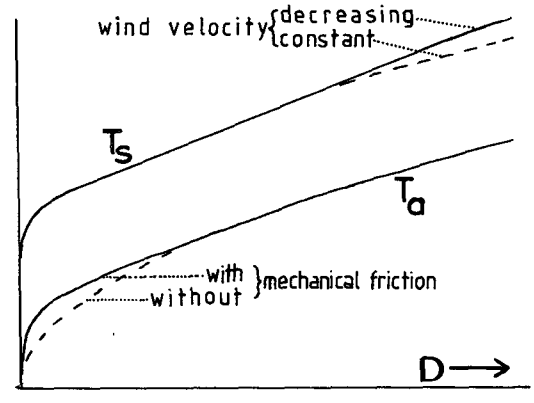

FIG. 3. Surface and air temperature as a function of distance to the sea. In its simplest form the slab-layer model results in a temperature increase proportional with the square root of distance. The mechanical friction term of Eq. (8) and a decreasing wind velocity inland result in a more linear increase of surface temperature.

are within the planetary boundary layer. The lowest layer is at 50 m above the surface.

The wind velocity is calculated from

$$\frac{\partial u}{\partial t} = -u\frac{\partial u}{\partial x} - \dot{\sigma}\frac{\partial u}{\partial \sigma} + f(v - v_g - v_g') - \frac{g}{p_*}\frac{\partial \tau_x}{\partial \sigma} + F_u, \tag{12}$$

$$\frac{\partial v}{\partial t} = -u\frac{\partial v}{\partial x} - \dot{\sigma}\frac{\partial v}{\partial \sigma} - f(u - u_g) - \frac{g}{p_*}\frac{\partial \tau_y}{\partial \sigma} + F_v, \tag{13}$$

where $\dot{\sigma} = d\sigma/dt$ (the σ vertical velocity); $\dot{\sigma}$ and relative pressure p_* follow from the vertically integrated continuity equation. Differential heating of the air above land and sea, based on a energy balance method, leads to a hydrostatic pressure adjustment. This yields an additional pressure gradient $\partial p_*/\partial x$ and geopotential gradient $\partial\Phi/\partial x$, which cause an additional geostrophic wind v_g':

$$v_g' = \frac{1}{f}\left(\frac{RT}{p_* + p_{\text{top}}/\sigma}\frac{\partial p_*}{\partial x} + \frac{\partial \Phi}{\partial x}\right). \tag{14}$$

Now v_g' provides an acceleration of the wind perpendicular to the coast, u, and through the term $f(u - u_g)$ an acceleration of v: the landbreeze or seabreeze effect. Finally v will approach $v_g + v_g'$.

The u component is very important for the temperature field over the heated land area since advection of relatively cool sea air is proportional to u. From Eq. (12) we see that differential horizontal and vertical advection also contribute to the u wind field. These components can be large in the vicinity of the sea breeze front. The term $-(g/p_*)\partial\tau/\partial\sigma$ represents vertical exchange of momentum by turbulent diffusion; this is particularly important in the boundary layer and depends strongly on the surface roughness z_0 and the stability of the boundary layer. Here z_0 is also important for the energy balance; we used a microscale roughness length: $z_0 = 0.03$ m. For the turbulent fluxes of momentum, heat and water vapor we use the parameterization of Louis (1979). The result of the turbulent diffusion is an Ekman layer in which the wind (and the horizontal advection) increases and veers with height. Finally horizontal diffusion, F_u and F_v, also influences the wind field; we use the five-point Shapiro (1970) operator.

Temperature and specific humidity are calculated from nonlinear advection equations like those for u and v; the mesoscale vertical motion field influences temperature by adiabatic warming/cooling. The surface fluxes are calculated in the same way as discussed in Section 2a. Over land, turbulent diffusion and dry convective adjustment cooperate in forming the mixed layer. Nonlinear advection and horizontal diffusion influence the fields too. For instance, the prolonged weak downward motion over sea caused by the sea breeze circulation causes a steady adiabatic warming of the air at some height over sea. Therefore in the afternoon somewhat less cold air is advected onshore than in the morning.

Now the magnitude of the time-integrated differential heating of the air over land and over sea determines the strength of the thermally driven circulation, and therefore we must start the calculations at a time with zero differential heating. In summer this is about 0700 local time. To calculate the fields at 1400 local time we thus need a 7 h simulation run. We initialize the model with a horizontal homogeneous temperature and specific humidity field based on the initial vertical temperature profile. At $t = 0$ the wind is in geostrophic balance, but dependent on σ in the boundary layer [Ekman profile, dependent on z_0 (sea) or z_0 (land)]. The surface temperature also is horizontally homogeneous at $t = 0$ and equals the sea surface temperature.

Compared to model 1, using the initial vertical temperature profile results in a decrease of the model sensitivity for measurement errors (see Section 2b). Further on models 2 and 3 compensate measurement errors in the following way: when the initial temperature difference $T_s - T_a$ is taken too high, the initial sensible heat flux is overestimated, resulting in a higher air temperature and a smaller error in the next flux calculation.

3. Data

As test area the grassland area of approximately 1000 km^2 in Friesland (6°E, 53°N) in the northern part of the Netherlands was selected. It is a flat area (maximum height 3 m above sea level) divided from the sea by a narrow strip of arable land (see Fig. 4). The area was chosen because of the homogeneity of the grassland and the underlying soil, and the absence of dunes.

Surface temperature measurements are obtained from the NOAA-7 satellite, which has a variable overpass time of about 1500 GMT (almost the same solar time). Data were obtained for eight days of summer 1983 with northerly winds and clear skies in the test area. One day is not analyzed as sea fog was flooding into the region.

Surface temperatures are calculated on the basis of the split-window technique (Prabakhara *et al.*, 1974). For open water McClain (1980) found that with a rms error of about 1°C over all oceans,

$$T_s = -10.78 + 1.035T(4) + 3.046[T(4) - T(5)], \tag{15}$$

where $T(x)$ is radiance temperature measured in AVHRR channel x. Although this algorithm is not verified for land surfaces, it is selected for the following reasons:

- The method is simple as compared to atmospheric absorption models.
- In this study we want to test models that assume atmospheric variability in the region, so an atmospheric absorption model should be run for different

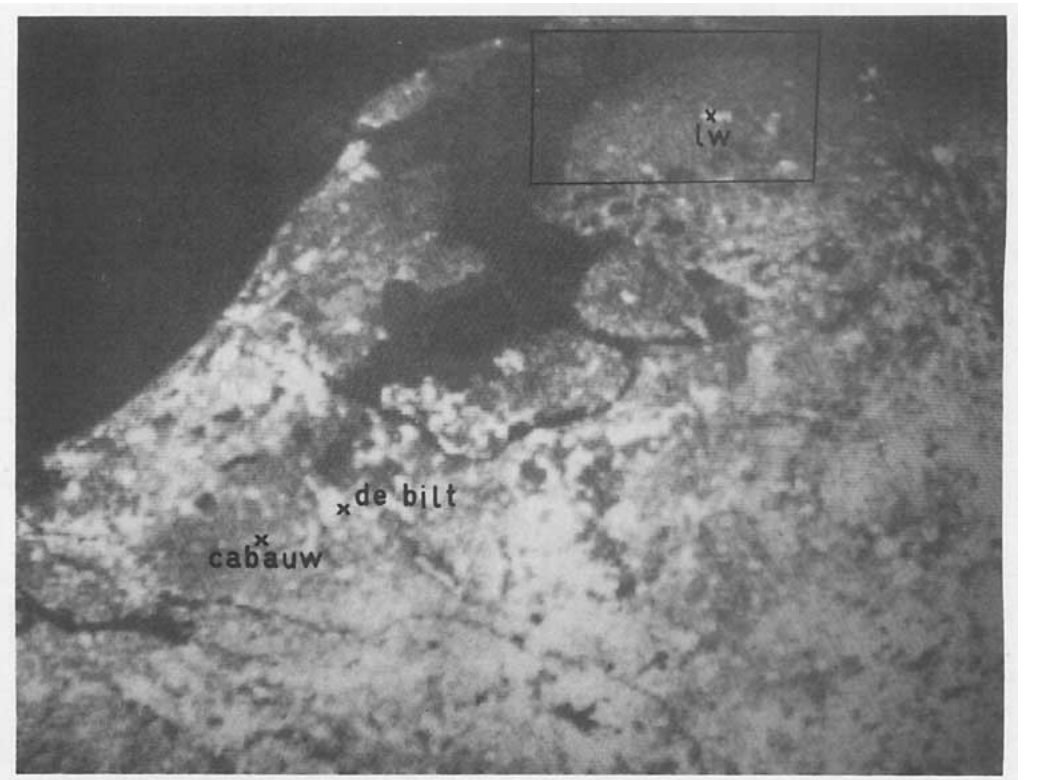

FIG. 4. Infrared picture of the test area (within the rectangle). Cold surface temperatures are black, warm temperatures white. Note the low temperatures near the coast (wind direction NE) and the high temperature at the city Leeuwarden (LW) in the middle of the test area.

atmospheric profiles. The split-window technique accounts for the variability of air temperature and humidity.

• Deviations between land and sea applications are probably small: The split-window technique is calibrated on buoys that measure water temperature just below the surface. Fortunately the surface temperature is only some tenths of a degree below the temperature of the water just below the surface (Clauss *et al.*, 1970; Liu *et al.*, 1979). Further on the emissivities of water and grassland agree remarkably well (see Table 1).

The atmospheric temperature profile was estimated from radiosonde measurements at the nearest station, De Bilt, situated some 130 km south of the test area. The temperature measurements show a strong diurnal cycle in the boundary layer (the first km above the surface). This diurnal cycle is not expected for the air flowing from the sea into the test area. Therefore the diurnal cycle is compensated by taking the average of the measurements of 1200 and 2400 GMT. It seems interesting to review the possibilities of using satellite soundings as input for the atmospheric temperature profile.

TABLE 1. Measured emissivities of water and grassland.

Author	Wavelength	Water	Grassland
Buettner and Kern (1965)	8–12 μm	0.993	0.988
Becker *et al.* (1980)	8–14 μm	0.981	0.989

Geostrophic wind, as calculated from the pressure gradients between several stations, also showed a strong diurnal cycle in the coastal zone. Therefore daily mean air pressure was used. Problems with this averaging method are expected when synoptic-scale air pressure changes much within one day and isallobaric effects should be taken into account.

Evapotranspiration is measured following the Bowen method by the Royal Netherlands Meteorological Institute at Cabauw (de Bruin and Holtslag, 1982), some 150 km south of the test area. Soil type (clay), groundwater level (−1 m) and vegetation (mainly grass) are similar to the test area. Therefore reasonable agreement between evapotranspiration at both sites may be expected.

Most measurements at Cabauw are performed using the so-called energy balance field. Unfortunately this field is more sensitive to drought than the surroundings. For that reason we used the Bowen-ratio measurements of a nearby field up to a height of 10 m. These measurements are expected to be more repre-

sentative for a larger area. So the evapotranspiration measurements that are used in this study are compounded from radiation and soil heat measurements at the energy balance field and the Bowen ratio of the neighboring fields.

Air temperature and wind velocity in the test area are observed at the meteorological station at the airport of Leeuwarden and at some amateur meteorologists' stations. The Leeuwarden data are used as input for model 1.

4. Results

Evapotranspiration according to Eq. (3) appears to be strongly dependent on the temperature difference between the surface and the air and on the wind velocity. Therefore we will first discuss temperatures and winds.

a. Wind velocity

The wind velocity as calculated with model 3 is shown in Fig. 5. A strong day-to-day variation is obvious and can be explained by differences in wind direction and differential surface heating. Averaged over all days a wind velocity drop in the first 30 km from the coast of only 0.08 m s^{-1} is found. As the test area is restricted to the first 30 km from the coast this result means that the assumption of constant wind velocity for models 1 and 2 is appropriate in the test area.

According to model 3 a wind velocity drop of 1.93 m s^{-1} is found in the region 30–50 km from the coast. The region of a sharp decrease in wind velocity starts in the morning at the coast and moves inland during the day. So the result of a constant wind velocity in the test area is fortuitous.

Calculated and measured wind data are compared. To distinguish measurement errors from erroneous calculations the following assumptions are made: Measurement errors are assumed to result from a deviating surface roughness near the meteorological

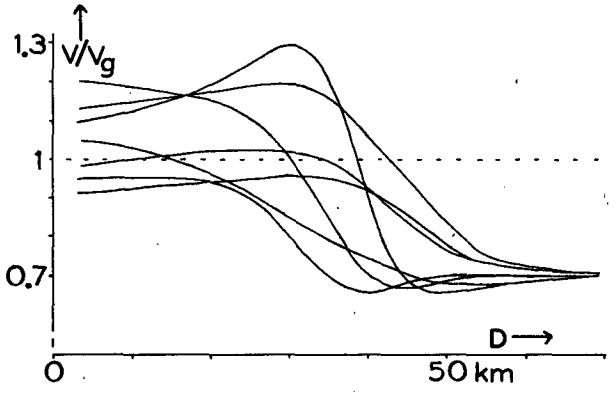

FIG. 5. Calculated wind velocity divided by geostrophic wind for all days of observation as a function of distance to the coast.

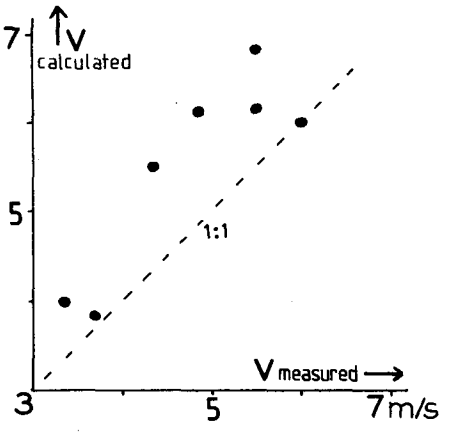

FIG. 6. Calculated versus measured wind velocity averaged over three meteorological stations for all days of observation.

station; so measurement errors of a certain station can be taken constant for all days of observation. Calculation errors are assumed to be constant over the test area, but may change from day to day. Then the following results are found.

The measurements show a scatter of only σ_{n-1} = 0.34 m s^{-1} around the calculated value. So wind measurement errors are small in the test area for the days of observation. To find the calculation errors, the average wind velocity at the three measurement stations has been taken; the result is shown in Fig. 6.

On average, calculated wind velocities are 0.76 m s^{-1} above measured data. To understand this difference we have to analyze the surface roughness in more detail. Measurements in Cabauw (van Ulden *et al.*, 1976) show that the roughness length for momentum flux is dependent on measurement height: At 1.1 m height z_0 = 0.02 m is found, but at 10 m height roughness length increased to z_0 = 0.2 m. Roughness length for momentum flux appears to depend on measurement height, since for increasing height rough obstacles such as trees in the surrounding area have a larger influence on the momentum exchange. This indicates that the mesoscale wind velocity should be calculated with a larger roughness length. With z_0 increasing from 0.03 to 0.2 m a wind velocity drop of 0.8 m s^{-1} is calculated with model 3 in the test area, in excellent agreement with observations. However, with z_0 = 0.2 m and known heat fluxes an erroneous surface temperature is calculated. This means that the wind velocity field should be calculated from the mesoscale surface roughness and the heat fluxes from the smaller roughness of the microscale elements!

The day-to-day scatter of Fig. 6 is σ_{n-1} = 0.54 m s^{-1}; the scatter is probably mainly caused by errors in the geostrophic wind that is used as input for model 3. Although the day-to-day scatter is low, it is above the scatter σ_{n-1} = 0.34 m s^{-1} of the meteorological stations. This is not in agreement with Warner

et al. (1983), who found a low areal homogeneity of the wind field. However, with our results, we conclude that for conditions of clear sky and low windspeed, surface observations of wind velocity are appropriate.

b. Surface temperature

The absolute value of surface temperature could not be verified in this study due to lack of ground measurements. Therefore, we will assume that the absolute accuracy of less than 1°C, found over water (McClain, 1980), is also valid over grass. In this section only the gradients of the observed surface temperatures are discussed.

Surface temperature is found to be strongly dependent on the distance to the sea. Parallel to the coast the temperature gradient was small. As a result an average surface temperature can be calculated as a function of the distance to the coast. Because of the averaging over 20–30 pixels the surface temperature could be determined with a low point-to-point scatter. Three typical profiles are shown in Figs. 7–9.

At 20 June the surface temperature of the arable land is about 2°C above the temperature of the grassland (Fig. 7). The July and August data do not show significant surface temperature differences between arable land and grassland (Fig. 8). An explanation of this feature is that in June some bare soil is still observed in the arable land. Because of the low surface roughness of bare soil, the sensible heat flux of the arable land may be overestimated with the June data. The June data resulted in a reduction of 20% in the calculated evapotranspiration of the arable land. The arable land heat fluxes are used as input for models 2 and 3 for the calculation of the vertical temperature profiles in the atmosphere. But as the strip of arable land is only 3–5 km wide, errors in the heat flux calculation of the arable land have a negligible influence on the resulting temperature profile above grassland.

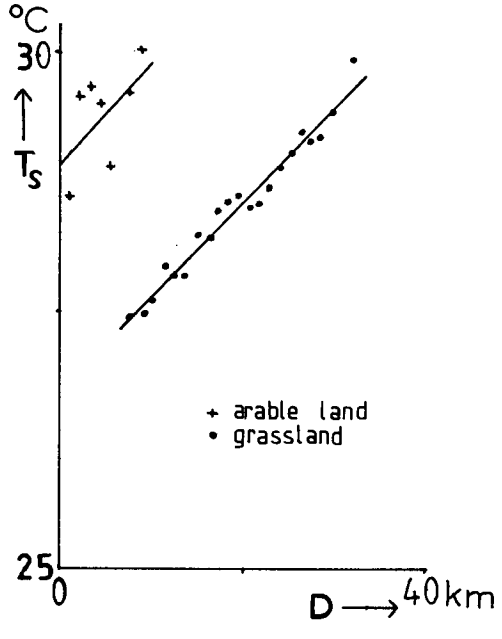

FIG. 7. Surface temperature as a function of distance to the sea in Friesland, 1444 GMT 20 June 1983.

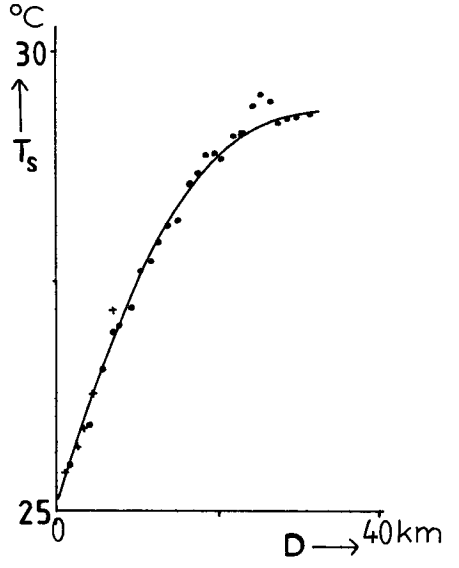

FIG. 8. As in Fig. 7 but for 1438 GMT 11 August 1983.

Surface temperatures on land near the coast were 5–10°C above the sea surface temperature. An interesting feature is that most pictures show an almost linear increase of surface temperature with distance from the sea. Sometimes even overshooting is observed (Fig. 9). Overshooting can be explained with model 3, in which a wind velocity minimum is calculated near the sea breeze front. The linearity of the surface temperature increase is explained in Section 2b3). So qualitatively the surface temperature observations agree well with model calculations.

c. Air temperature

Air temperature is calculated with models 2 and 3. As both model results show close agreement for air temperature, only model 2 results are discussed in this section. As for wind velocity, we will assume that day-to-day differences between measurements and calculations are caused by erroneous calculations, and that systematic station-to-station differences are caused by nonrepresentativeness of the measurement station. Again it is assumed that air temperature is constant parallel to the coast.

The average of air temperature for all days is shown in Fig. 10. The calculated increase of air temperature is in good agreement with observations. On average the calculated air temperature is 0.76°C above the observations. This difference is probably caused by

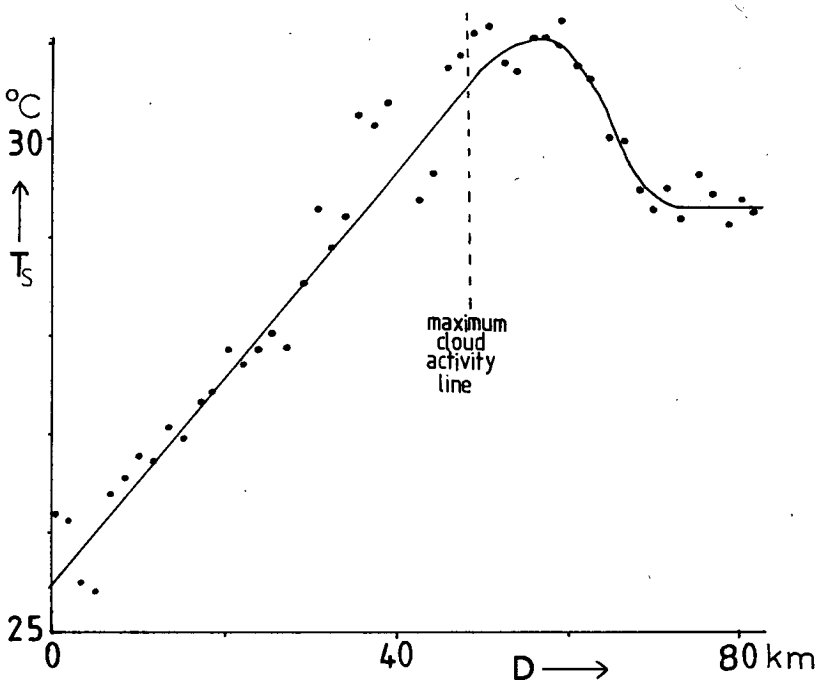

FIG. 9. As in Fig. 7 but for Belgium with a sea-breeze circulation.

errors in the initial vertical temperature profile that is used as input for models 2 and 3. Averaged for all days, the observations show a scatter of $\sigma_{n-1} = 0.84°C$ around the calculated air temperature. This systematic scatter between the meteorological stations is probably not caused by instrumental errors, but by station-to-station variations of true air temperature that are due to variable surface properties (see section 2b, model 1).

Averaged for all meteorological stations, the calculated air temperature shows a day-to-day scatter of 0.66°C (see Fig. 11). The largest overestimation is found for low air temperatures, but this feature is probably accidental.

It is concluded that the air temperature is calculated with a lower day-to-day scatter than station-to-station

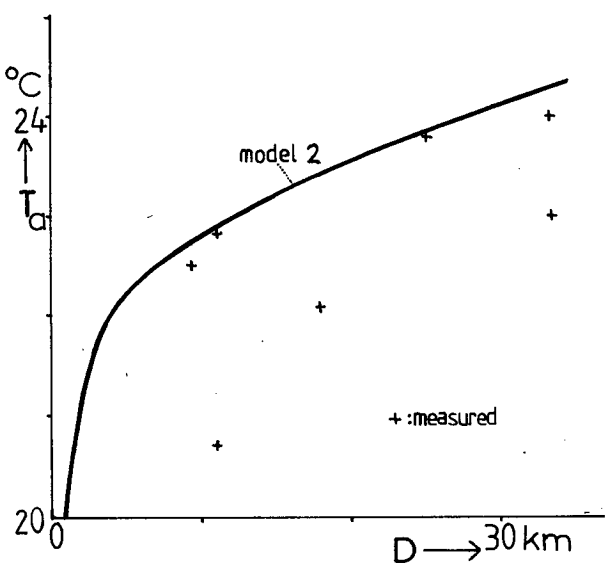

FIG. 10. Air temperature versus distance to the sea, averaged for all days of observation. The lowest air temperatures were found at Leeuwarden airport, used for model 1 calculations.

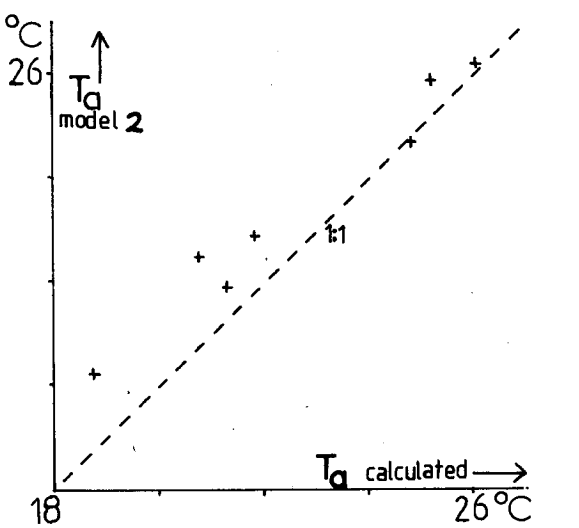

FIG. 11. Calculated versus measured air temperature averaged for all meteorological stations.

scatter (0.66 and 0.84°C, respectively), but the differences are small. Because of the low scatter, both observed and calculated air temperature are suitable for the calculation of the heat fluxes. However because of the strong increase of air temperature with distance to the sea the model 1 assumption of constant air temperature is not realized in the test area.

d. Evapotranspiration

Evapotranspiration is calculated with the models and compared with ground measurements. It must be kept in mind that the measurements were taken 150 km south of the test area, resulting in different meteorological and surface conditions. The results are also compared with the Priestley–Taylor evapotranspiration E_{pt} (Eq. 6) with $\alpha = 1$ and $\beta = 20$ W m^{-2} as found by de Bruin and Holtslag (1982) for average Netherlands summer conditions. As an average, measured evapotranspiration appeared to be 65 W m^{-2} (or 21%) below E_{pt}, indicating that during the test days the soil was dryer than for average summer conditions.

1) MODEL 1

Evapotranspiration is calculated with the surface temperatures of the grassland surroundings of the Leeuwarden meteorological station, and is 82 W m^{-2} below measurements with a scatter $\sigma_{n-1} = 37$ W m^{-2} (Fig. 12). The underestimation of model 1 can essentially be explained by the nonrepresentativeness of the meteorological station, which showed maximum deviation with the calculated air temperature (Fig. 10). The reference station is situated behind the runway of the airport, resulting in a roughness length of only $z_0 = 0.01$ m for the prevailing wind direction (Wieringa and van der Veer, 1976). However it seems unlikely that the underestimation of the air temperature is as much as 2.2°C. Therefore, we believe that

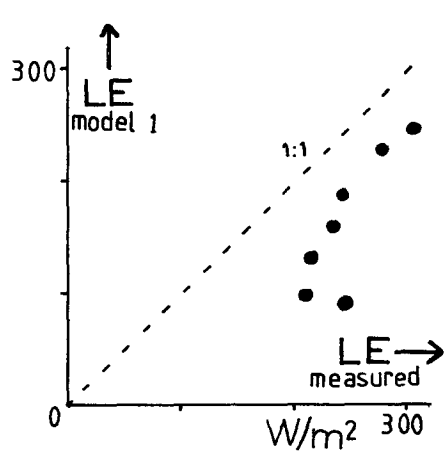

FIG. 12. Model 1 versus measured evapotranspiration for the test days.

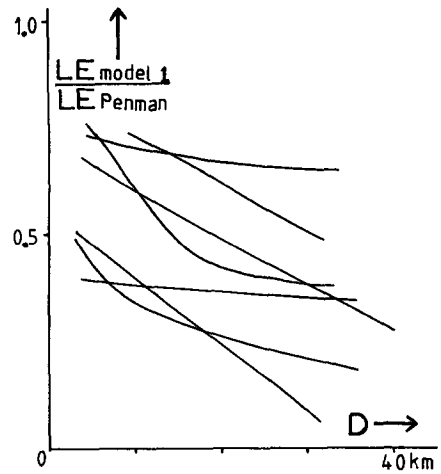

FIG. 13. Model 1 evapotranspiration scaled with the Priestley–Taylor value versus distance to the sea.

part of the underestimation is caused by underestimation of the vegetation resistance r_v ([Eq. (5)]. This might also explain why the largest deviations in Fig. 12 are found for low fluxes of evapotranspiration or high fluxes of sensible heat.

Evapotranspiration versus distance to the sea is shown in Fig. 13. The assumptions of constant air temperature and wind velocity result in a decrease of 65 ± 36 W m^{-2} between 6 and 30 km from the coast. By assuming a constant air temperature at 2 m height the calculated decrease would be some 50% higher! For such a homogeneous area the calculated flux gradient is believed to be unacceptable, showing that variations of air temperature must be taken into account.

2) MODEL 2

On average, model 2 is only 7 W m^{-2} below observations with a rms scatter of 34 W m^{-2} (Fig. 14). Except for one day, the agreement is remarkably close, but this agreement is probably caused by coincidental cancellation of errors in the initial temperature profile, the vegetation resistance r_v [Eq. (5)] and the representativeness of the measured evapotranspiration for our test area.

Model 2 shows an areal constant evapotranspiration: LE (6 km) − LE (30 km) = 0 ± 30 W m^{-2} (Fig. 15), showing that the assumption of constant wind velocity (Fig. 5) and the method of calculating the increase of air temperature (Fig. 10) are suitable in the test area.

3) MODEL 3

On average model 3 is only 1 W m^{-2} below measurements but with a relatively high rms scatter (73 W m^{-2}), compared to model 2 (Fig. 16). The same holds for the areal dependence: LE (6 km)

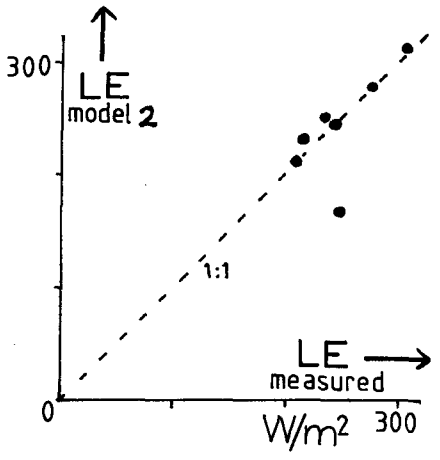

FIG. 14. Model 2 versus measured evapotranspiration.

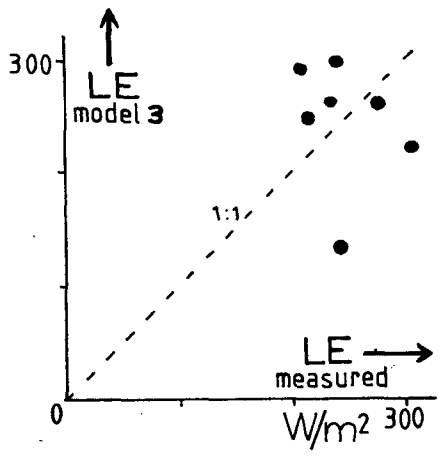

FIG. 16. As in Fig. 12 but for model 3 calculations.

$-LE$ (30 km) = -11 ± 42 W m^{-2} (Fig. 17). The increased scatter is explained by inaccuracies in the geostrophic wind used as input for model 3 (see Section 4a). The scatter can be decreased by calibration of the geostrophic wind on measured wind velocities.

5. Conclusions

Derivation of evapotranspiration from surface temperatures requires accurate input data of the wind velocity and the temperature difference between surface and air. It is shown that for flux calculations the sea surface temperature is measured with sufficient accuracy from satellite observations, using the split-window technique. It is plausible that the same technique can be used to calculate surface temperatures of grassland. Therefore this study concentrates on the air temperature and wind velocity.

From a theoretical discussion it is concluded that temperature and wind at a height of 2 m are strongly affected by the fluxes of the underlying surface. So for flux calculations the assumption of constant wind and temperature at 2 m height is inappropriate. On a microscale the assumption of constant atmospheric properties is better realized at the base of the mixed layer, some tens of meters above the surface. Although the constant flux layer generally does not reach the mixed layer, it is acceptable to use the flux-profile relations up to the mixed layer. With this approach, the surface fluxes are less sensitive to temperature differences and measurement errors. By assuming horizontally constant air properties at only 2 m height, a serious overestimation of evapotranspiration differences would be the result!

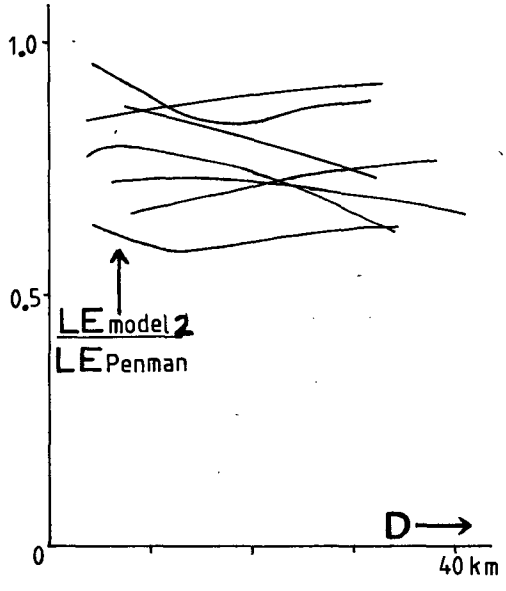

FIG. 15. As in Fig. 13 but for model 2 calculations.

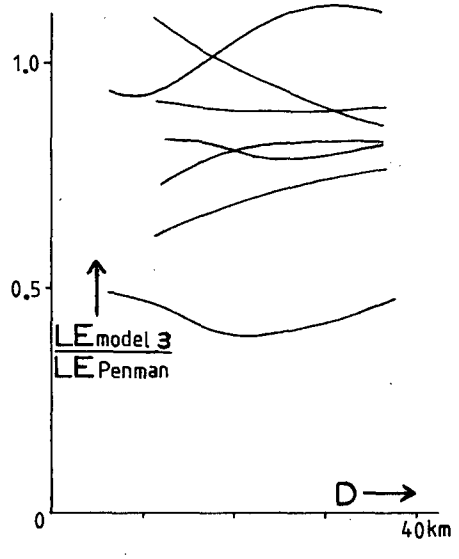

FIG. 17. As in Fig. 13 but for model 3 calculations.

Since temperature and wind near the bottom of the mixed layer are normally not measured, three models have been used to calculate these values over the test area. By comparing the results, we found that in our case the wind velocity could be taken constant over the test area. With cold air advection from the sea the mixed layer temperature has to be varied with distance to the sea. The temperature variation in the mixed layer could well be calculated with a simple slab-layer model using an initial atmospheric temperature profile. For two reasons such models are less dependent on measurement errors of temperature: the model uses air temperatures from a greater height and it compensates errors after time integration. Therefore such models are recommended for flux calculations from surface temperatures.

From the atmospheric temperature profile, evapotranspiration is calculated with model 2 with a rms error of only 34 W m^{-2} and neglectable bias. This result is well within the accuracy of the surface observations when extrapolated to the test area. This indicates that satellite observations of surface temperatures can be used not only to predict evapotranspiration differences, but also to determine the absolute value of evapotranspiration! With the Priestley–Taylor approach using tuning factors for average Netherlands summer conditions a bias of 65 W m^{-2} was found. So model 2 may be used to tune the Priestley–Taylor scheme for interpolation of evapotranspiration between succeeding satellite observations.

Although some measurements were made outside the test area and the study is restricted to one limited area, we recommend further verification of this method.

Acknowledgments. The investigations were supported by the Department of Education and Science, through its Division of Science Policy. The authors acknowledge Prof. C. J. E. Schuurmans and Dr. H. A. R. de Bruin (KNMI) for creative discussions, W. Kohsiek (KNMI), P. Baylis (Dundee), F. Ynsen, J. Dijkstra, F. van Dijk, A. van der Lee, J. D. Bakker, R. Flapper and G. Dorenbos for data supply, Dr. J. van Kats and Dr. F. van der Linden for data handling and M. A. de Haan for typing the manuscript.

APPENDIX

Calculation of the Energy Balance from Standard Weather Data

The energy balance equation (1) is calculated according to Holtslag and van Ulden (1983), except for the distribution between sensible and latent heat flux, which is discussed in text Section 2a.

As net radiation may have a large areal variation, it is calculated from the incoming solar shortwave (K), and longwave (L) radiation by:

$$Q = (1 - a)K + \epsilon(L - \sigma T_s^4). \quad \text{(A1)}$$

The surface albedo can be calculated from the satellite observations (Mekler and Joseph, 1983), but in this study $a = 0.23$ was used for grassland. Further on we used as emissivity $\epsilon = 0.98$ and the Stephan–Boltzmann constant $\sigma = 5.67 \times 10^{-8}$ W m^{-2} K^{-4}. Incoming solar radiation is calculated from solar elevation ϕ with cofficients of Collier and Lockwood (1974):

$$K = 990 \sin\phi - 30. \quad \text{(A2)}$$

Incoming longwave radiation can be calculated from air temperature and humidity. But as air temperature and humidity are well correlated for Dutch summer conditions, we may as well use the Swinbank (1963) relation:

$$L = 5.31 \times 10^{-13} T_a^6, \quad \text{(A3)}$$

where T_a is measured at 2 meters. Finally, soil heat flux is estimated by de Bruin and Holtslag, (1982):

$$G = 0.1Q. \quad \text{(A4)}$$

REFERENCES

Anthes, R. A., and T. T. Warner, 1978: Development of hydrodynamic models suitable for air pollution and other mesometeorological studies. *Mon. Wea. Rev.*, **106,** 1045–1078.

Bartholic, J. F., L. N. Namken and C. L. Weigand, 1972: Aerial thermal scanner to determine temperatures of soils and crop canopies differing in water stress. *Agron. J.*, **64,** 603–608.

Becker, F., W. Ngai and M. Stoll, 1980: An active method for measuring thermal infra-red effective emissivities. Implications and perspectives for remote sensing. *COSPAR*, Budapest, 193–210.

Bruin, H. A. R. de, and A. A. M. Holtslag, 1982: A simple parameterization of the surface fluxes of sensible and latent heat during daytime compared with the Penman–Monteith concept. *J. Appl. Meteor.*, **21,** 1610–1621.

Buettner, K. J. K., and C. D. Kern, 1965: The determination of infrared emissivities of terrestrial surfaces. *J. Geophys. Res.*, **70,** 1329–1336.

Carlson, T. B., J. K. Dodd, S. G. Benjamin and J. N. Cooper, 1981: Satellite estimation of the surface energy balance, moisture availability and thermal inertia. *J. Appl. Meteor.*, **20,** 67–87.

Clauss, E., H. Hinzpeter and J. Mueller-Glewe, 1970: Messungen zur Temperatur-struktur im Wasser an der Grenzfläche Ozean–Atmosphäre. *Meteor. Forsch. Ergebnisse,* Reihe **B.,** 90–94.

Chou, S. H., and D. Atlas, 1982: Satellite estimates of ocean–air heat fluxes during cold air outbreak. *Mon. Wea. Rev.*, **110,** 1434–1450.

Collier, L. R., and J. G. Lockwood, 1974: The estimation of solar radiation under cloudless skies with atmospheric dust. *Quart. J. Roy. Meteor. Soc.*, **100,** 678–681.

——, and ——, 1975: Reply. *Quart. J. Roy. Meteor. Soc.*, **101,** 390–392.

Deardorff, J. W., 1972: Parameterisation of the boundary layer for use in general circulation models. *Mon. Wea. Rev.*, **100,** 93–106.

Driedonks, A. G. M., 1982: Models and observations of the growth of the atmospheric boundary layer. *Bound-Layer Meteor.*, **23,** 283–306.

England, C. E., R. Gombeer, E. Hechinger, R. W. Herschy, A. Rosema and L. Stroosnijder, 1983: The Group Agromet Monitoring Project (GAMP): Application of Meteosat data for rainfall, evaporation, soil-moisture and plant-growth monitoring in Africa. *ESA Journal* **7,** 169–188.

Gurney, R. J., and D. K. Hall, 1983: Satellite derived surface

energy balance estimates in the Alaskan sub-arctic. *J. Climate Appl. Meteor.*, **22,** 115–125.

Holtslag, A. A. M., and A. P. van Ulden, 1983: A simple scheme for daytime estimates of the surface fluxes from routine weather data. *J. Climate Appl. Meteor.*, **22,** 517–529.

Idso, S. B., T. J. Schmugge, R. D. Jackson and R. J. Reginato, 1975: The utility of surface temperature measurements for the remote sensing of soil water status. *J. Geophys. Res.*, **80,** 3044–3049.

Jackson, R. D., R. J. Reginato and S. B. Idso, 1977: Wheat canopy temperature: A practical tool for evaluating water requirements. *Water Resour. Res.*, **13,** 651–662.

Klaassen, W., 1980: Mapping of soil water status from thermal infrared remote sensing. EARS, Delft, 48 pp. (in Dutch).

——, and G. J. A. Nieuwenhuis, 1978: Estimation of the regional evapotranspiration from remotely sensed crop surface temperatures: Arable land. *Nota* 1057, ICW, Wageningen, 29 pp.

Liu, W. T., K. B. Katsaros and J. A. Businger, 1979: Bulk parameterization of air–sea exchanges of heat and water vapor including the molecular constraints at the interface. *J. Atmos. Sci.*, **36,** 1722–1734.

Louis, J. F., 1979: The parameterization of the planetary boundary layer. ECMWF, Lecture note 9, 29 pp.

McClain, E. P., 1980: Multiple atmospheric window techniques for satellite-derived sea surface temperatures. *Oceanography from Space,* J. F. R. Grower, Ed., Plenum Press, 73–85.

Mekler, Y., and J. H. Joseph, 1983: Direct determination of surface albedos from satellite imagery. *J. Climate Appl. Meteor.*, **22,** 530–536.

Pasquill, F., 1972: Some aspects of boundary layer description. *Quart. J. Roy. Meteor. Soc.*, **98,** 469–494.

Prabhakara, C., G. Dalu and V. G. Kunde, 1974: Estimation of sea surface temperature from remote sensing in the 11 μm to 13 μm window region. *J. Geophys. Res.*, **79,** 5039–5044.

Price, J. C., 1982: On the use of satellite data to infer surface fluxes at meteorological scales. *J. Appl. Meteor.*, **21,** 1111–1122.

Reiff, J., D. Blaauboer, H. A. R. de Bruin, A. P. van Ulden and G. Cats, 1984: An air-mass transformation model for short range weather forecasting. *Mon. Wea. Rev.*, **112,** 393–412.

Seguin, B., and B. Itier, 1983: Using midday surface temperature to estimate daily evaporation from satellite thermal IR data. *Int. J. Remote Sens.*, **4,** 371–383.

Shapiro, R., 1970: Smoothing, filtering and boundary effects. *Rev. Geophys. Space Phys.*, **8,** 359–387.

Soer, G. J. R., 1980: Estimation of regional evapotranspiration and soil moisture conditions using remotely sensed crop surface temperatures. *Remote Sens. Environ.*, **9,** 27–36.

Stage, S. A., 1983: Boundary layer evolution in the region between shore and cloud edge during cold air outbreaks. *Mon. Wea. Rev.*, **111,** 1453–1471.

Swinbank, W. C., 1963: Long-wave radiation from clear skies. *Quart. J. Roy. Meteor. Soc.*, **89,** 339–348.

Tennekes, H., 1973: A model for the dynamics of the inversion above a convective layer. *J. Atmos. Sci.*, **30,** 558–567.

Thom, A. S., 1972: Momentum, mass and heat exchange of vegetation. *Quart. J. Roy. Meteor. Soc.*, **98,** 124–134.

Ulden, A. P. van, J. G. van Vliet and J. Wieringa, 1976: Temperature and wind observations at heights from 2 to 200 m at Cabauw 1973. KNMI, Scientific Rep. 76-7, 17 pp.

Warner, T. T., R. R. Fizz and N. L. Seaman, 1983: A comparison of two types of atmospheric transport models—Use of observed winds versus dynamical predicted winds. *J. Climate Appl. Meteor.*, **22,** 394–406.

Wetzel, P. J., D. Atlas and R. H. Woodward, 1984: Determining soil moisture from geosynchronous satellite infrared data: A feasibility study. *J. Climate Appl. Meteor.*, **23,** 375–391.

Wieringa, J., 1980: Representativeness of wind observations at airports. *Bull. Amer. Meteor. Soc.*, **61,** 962–971.

——, and P. J. M. van der Veer, 1976: Dutch windstations 1971–1974. KNMI, V 278, 90 pp (in Dutch).